PROGRESS IN INORGANIC CHEMISTRY

Edited by

KENNETH D. KARLIN

DEPARTMENT OF CHEMISTRY
JOHNS HOPKINS UNIVERSITY
BALTIMORE, MARYLAND

VOLUME 55

WILEY-INTERSCIENCE
A John Wiley & Sons, Inc., Publication

This Page Intentionally Left Blank

Progress in Inorganic Chemistry

Volume 55

Advisory Board

PROGRESS IN INORGANIC CHEMISTRY

Edited by

KENNETH D. KARLIN

DEPARTMENT OF CHEMISTRY
JOHNS HOPKINS UNIVERSITY
BALTIMORE, MARYLAND

VOLUME 55

WILEY-INTERSCIENCE
A John Wiley & Sons, Inc., Publication

Published by John Wiley & Sons, Inc., Hoboken, New Jersey
Published simultaneously in Canada

Library of Congress Catalog Card Number 59-13035
ISBN 978-0-471-68242-4

Printed in the United States of America

10 9 8 7 6 5 4 3 2 1

Contents

CHAPTER 1

Elucidation of Electron- Transfer Pathways in Copper and Iron Proteins by Pulse Radiolysis Experiments

OLE FARVER

Institute of Analytical Chemistry, University of Copenhagen, 2100 Copenhagen, Denmark

ISRAEL PECHT

Department of Immunology, The Weizmann Institute of Science, 76100 Rehovot, Israel

CONTENTS

Progress in Inorganic Chemistry, Vol. 55 Edited by Kenneth D. Karlin

I. INTRODUCTION

A. Biological Electron Transfer

Electron-transfer (ET) reactions play a central role in all biological systems ranging from energy conversion processes (e.g., photosynthesis and respiration) to the wide diversity of chemical transformations catalyzed by different enzymes (1). In the former, cascades of electron transport take place in the cells where multicentered macromolecules are found, often residing in membranes. The active centers of these proteins often contain transition metal ions [e.g., iron, molybdenum, manganese, and copper ions] or cofactors as nicotinamide adenine dinucleotide (NAD) and flavins. The question of evolutionary selection of specific structural elements in proteins performing ET processes is still a topic of considerable interest and discussion. Moreover, one key question is whether such structural elements are simply of physical nature (e.g., separation distance between redox partners) or of chemical nature (i.e., providing ET pathways that may enhance or reduce reaction rates).

Biological ET is characterized by the use of redox centers that are spatially fixed in macromolecules and thus separated by the protein matrix and usually prevented from coming in direct contact with solvent. Therefore intramolecular ET becomes a central part of the biological function of the redox proteins, and the ET rates are expected to decrease exponentially with the separation distance of the redox centers that is generally quite large ($>$1.0 nm). Further, usually only very modest structural changes of the active centers accompany the redox changes, thus minimizing the activation energy required for ET.

During the last decades there has been a remarkable progress in determination of three-dimensional (3D) structures of proteins, including many involved in ET, which has opened the way for a detailed study of the relationship between structure and reactivity of this large and diverse group of molecules (2).

A key challenge in studies of biological redox processes is trying to define and understand the parameters that control the rates of ET. These parameters include (a) driving force (i.e., change in free energy of the reaction); (b) the reorganization energy (i.e., the energy of the reactants at the equilibrium nuclear configuration of the products); (c) the distance separating electron donor and acceptor; and finally (d) the nature of the medium separating the two redox centers.

This chapter reviews results and current insights emerging primarily from pulse radiolysis (PR) studies of intramolecular ET in multisite proteins, mainly iron- and copper-containing redox enzymes, with emphasis on interactions between the different redox centers.

B. Electron-Transfer Theory

Rates of ET are expected to depend on the energy required for bond-length and bond-angle changes of the reactants, as well as solvent reorganization accompanying the ET process. In proteins, however, these processes involve the polypeptide matrix as part of the medium that is far less homogeneous than solvent molecules surrounding small molecule ET partners. Further, conformational changes preceding or following ET in macromolecules may affect the free energy changes of the reaction. Moreover, while small molecules exchange electrons in solutions where they are in close, sometimes direct contact, in proteins the redox reaction partners are held in fixed positions by and within the polypeptide matrix. Hence, they are prevented from coming into direct inner-sphere contact. Therefore, the distance between electron donor and acceptor is one decisive parameter affecting long-range ET (LRET) rates. Considerable efforts have been devoted to studies of these processes, and the comprehension of intra- and interprotein mediated ET reactions has advanced significantly, largely due to the determination of 3D structures of an ever-increasing number of redox proteins. In addition, the theoretical models for analyzing LRET have also advanced to a stage where they can more readily be employed and tested experimentally. Still, some very interesting questions remain to be answered: (1) How does the ET rate depend on the nature of the medium separating the two redox partners in a protein system? (2) To what extent did the structures of redox proteins undergo evolutionary selection in order to optimize their function for specificity and control of biological ET, and if so, what are the structural corollaries of this selection? These are some of the issues that will be addressed in this chapter.

Several excellent reviews on ET theory are available (3–5). Here only an outline, necessary for the discussion of this topic, is presented. Long-range ET

in proteins is characterized by a weak interaction between electron donor, D, and acceptor, A, and in the nonadiabatic limit, where the D–A distance is large (>1.0 nm), the rate constant is proportional to the square of the electronic coupling between the electronic states of reactant and product, represented in the form of a tunneling matrix element, H_{DA}. For intramolecular ET the rate constant is given by Fermi's golden rule (3):

$$k = \frac{2\pi}{\hbar} H_{DA}^2 \cdot (FC) \tag{1}$$

The Franck–Condon factor (FC) for nuclear movements can for relatively small vibrational frequencies, where $k_B T > h\nu$, be treated classically, a condition that often applies to biological ET. In polar solvents like water, the reorientation of solvent molecules contributes considerably to the total reorganization energy, λ_{tot}, in response to changes in charge distribution of the reaction partners. The reorganization energy can be defined as the energy of the reactants at the equilibrium nuclear configuration of the products (3, 4). If D and A are viewed as conducting spheres, the dielectric model illustrates an important feature, namely, that the more polar the medium, the larger becomes λ_{tot} (3). Therefore, reorganization energy requirements are expected to decrease dramatically when the redox centers reside in a low-dielectric medium, (e.g., the hydrophobic interior of a protein). In a nonpolar environment, the reorganization energy requirement for the surrounding medium vanishes. Another contribution to the reorganization energy comes from changes in bond lengths and angles of the coordination sphere that accompany ET. The nuclear factor also expresses the relationship between reorganization energy and driving force that further influences the ET rate (cf. Eq. 2). The other factor included in the FC term is the driving force of the ET reaction that is given by the difference in reduction potentials of electron acceptor and donor. These potentials are rather sensitive to the structure and environment of the metal site and may thus be tuned by subtle conformational changes.

The electronic motion, however, requires a quantum mechanical approach, and the semiclassical Marcus equation may be expressed as (3):

$$k = \frac{2\pi}{\hbar} \frac{H_{DA}^2}{(4\pi\lambda_{tot} RT)^{\frac{1}{2}}} e^{-(\Delta G^\circ + \lambda_{tot})^2/(4\lambda_{tot} RT)} \tag{2}$$

where ΔG° is the reaction free energy and λ the nuclear reorganization energy. Since wave functions decay exponentially with distance, the tunneling matrix element, H_{DA} will decrease with the distance, $(r - r_0)$, as:

$$H_{DA} = H_{DA}^0 \cdot e^{-\beta(r-r_0)/2} \tag{3}$$

where H_{DA}^{0} is the electronic coupling at direct (van der Waals) contact between electron donor and acceptor (where $r = r_0$) and the decay rate of electronic coupling with distance is determined by the coefficient, β. In LRET, there is no direct electronic coupling between D and A. Instead, the coupling is mediated by the electronic states of the intervening atoms via superexchange. Both theoretical and experimental studies demonstrate that the chemical nature and structure of the protein medium separating electron donor and acceptor must be included in a theoretical analysis of the electronic coupling, H_{DA}, of the redox centers. In one theoretical treatment that has proven to be very useful (6, 7), the protein medium is divided into small elements linked by covalent bonds, hydrogen bonds and through-space contacts, and each type of link is then assigned a coupling decay factor (with distances in nm):

$$\begin{aligned} \varepsilon_C &= 0.6 \\ \varepsilon_H &= \varepsilon_C^2 \cdot \exp[-17(r - 0.28)] \\ \varepsilon_S &= 1/2\varepsilon_C \cdot \exp[-17(r - 0.14)] \end{aligned} \tag{4}$$

for covalent (C), hydrogen bonded (H), and van der Waals interaction (S). The ET pathways may now be identified by analyzing the bonding interactions that maximize H_{DA}, which now can be expressed as:

$$H_{DA} = P \cdot \prod_i \varepsilon_{C(i)} \prod_j \varepsilon_{H(j)} \prod_k \varepsilon_{S(k)} \tag{5}$$

The prefactor, P, depends on the electronic coupling of donor and acceptor with the bridging orbitals. A correlation between β (cf. Eq. 3) and ε_C (Eq. 4) is easily demonstrated: An individual strand of a β-sheet protein defines a linear tunneling pathway along the peptide, spanning a distance $(r - r_0)$ of 0.34 nm per residue (three covalent bonds). Thus, inserting a β value of 10 nm^{-1} in Eq. 3, the decay factor, ε_C of Eq. 4 becomes 0.6 per covalent bond.

The activation enthalpy is related to the thermodynamic parameters (3):

$$\Delta H^{\neq} = \frac{\lambda}{4} + \frac{\Delta H^{\circ}}{2}\left(1 + \frac{\Delta G^{\circ}}{\lambda}\right) - \frac{(\Delta G^{\circ})^2}{4\lambda} \tag{6}$$

The entropy of activation includes a contribution from the distance dependence of the electronic coupling (3) (cf. Eq. 3):

$$\Delta S^{\neq} = \Delta S^{*} - R\beta(r - r_0) \tag{7}$$

where β is the electronic coupling decay factor, and ΔS^{*} is related to the standard entropy change, ΔS° (3):

$$\Delta S^{*} = \frac{1}{2}\Delta S^{\circ}(1 + \Delta G^{\circ}/\lambda) \tag{8}$$

Particularly β-sheet proteins, being composed of extended polypeptide chains interconnected by hydrogen bonds, give rise to coupling pathways along the peptide backbone. Many studies have demonstrated that the distance decay constant, β, is $\sim 10\,\mathrm{nm}^{-1}$ (8). Using edge-to-edge separation distances between ligands involves some ambiguity since it is often difficult to define the atoms that comprise the edges of a donor and an acceptor. Experimental evidence now supports the notion that metal–metal distances are more appropriate (4) and this is the length scale employed here. In conclusion, the folded polypeptide, which constitutes the scaffold for the metal ion coordination sphere and provides the path for electron tunneling, plays the major role in determining the thermodynamic and electronic properties, and hence ET reactivity of a given pair of redox centers.

II. PULSE RADIOLYSIS

The main method employed in our studies described here is PR (9). Introduced and developed in the early 1960s, PR has found a broad range of important applications in both chemistry and biochemistry. Of considerable significance and interest are PR studies of ET processes in proteins. The method is based upon excitation and decomposition of solvent molecules by short pulses (typically 0.1–1 μs) of high energy (2–10 MeV) accelerated electrons yielding several primary products that can be employed for induction of additional reactions. Thus, though PR is essentially a higher energy analogue of flash photolysis, the latter method uses photoexcitation of specific solutes rather than bulk solvent, which distinguishes the two methods and provides the former with some clear advantages. For example, as the solvent is the source of the reactive species and no chromophore is required, essentially any reaction partner for the radicals formed can be chosen.

Different types of electron accelerator systems have been adopted for pulse radiolysis (10). In biochemical studies, pulsed electron accelerators have most often been used; these instruments produce short pulses of accelerated electrons with adequate energy to ensure uniform irradiation of the solution. The most common and versatile detection system is optical absorption, although other techniques have also been applied, including electrical conductivity, resonance Raman spectroscopy, or electron paramagnetic resonance (EPR) (11). When using optical detection, the analytical light beam is directed through the sample in a quartz cuvette perpendicular to the electron beam. After passing through the irradiated solution, the light beam is guided through a system of mirrors and lenses to a monochromator isolated from the radiation zone by a protective wall. Light of a selected wavelength then reaches the photomultiplier and the signal is finally transferred to a computer system via an analog–digital converter for further processing.

Introducing the electron pulses into dilute aqueous solutions under anaerobic conditions causes, as stated above, primary changes in the solvent (12). In such experiments, water molecules undergo conversion mainly into OH radicals and hydrated electrons [e^-(aq)] and, to a lesser extent, H atoms, H_2 and H_2O_2 molecules.

Yields of the reaction products are usually presented as G values giving the number of chemical species produced per 100 eV of absorbed energy: $G(e^-(aq)) = 2.9$; $G(OH) = 2.8$; $G(H) = 0.55$; $G(H_2) = 0.45$; $G(H_2O_2) = 0.75$ (12).

The hydrated electron and the hydroxyl radical are exceptionally reactive and present thermodynamic extremes of reducing and oxidizing potentials, respectively. These primary products, though having their own applications, are usually converted into less reactive and more selective agents using protocols devised by radiation chemists (12). Hence, they provide the possibility of inducing a wide range of ET processes, as illustrated by one useful procedure transforming e^-(aq) [with a reduction potential, $E^\circ = -2.8$ V vs. standard hydrogen electrode (SHE)] into a milder reductant, the CO_2^- radical ($E^\circ = -1.8$ V vs. SHE) (13). First, the hydrated electrons are converted into an additional equivalent of OH radicals by the following reaction in N_2O saturated solutions:

$$e^-(aq) + N_2O + H_2O \rightarrow N_2 + OH + OH^- \tag{9}$$

Second, the 2 equiv of OH radicals, as well as the hydrogen atoms, then react with formate anions to produce the CO_2^- radical in a diffusion-controlled process:

$$HCO_2^- + OH/H \rightarrow H_2O/H_2 + CO_2^- \tag{10}$$

By analogy, other reducing and oxidizing radicals can be produced by similar protocols. Thus, uncharged 1-methylnicotinamide radicals (1-MNA*), which are formed by the following reaction sequence, have also been employed: The OH radicals are scavenged by *tert*-butanol to produce a relatively inert radical species that hardly reacts with copper- or heme containing proteins:

$$OH + Me_3OH \rightarrow H_2O + \cdot CH_2Me_2OH \tag{11}$$

1-methylnicotinamide chloride (1-MNA^+ Cl^-) reacts with solvated electrons to produce 1-MNA* with a reduction potential, $E^0 = -1.0$ V vs. SHE (13):

$$\text{1-}MNA^+ + e^-(aq) \rightarrow \text{1-}MNA^* \tag{12}$$

The choice of radicals to be employed for reaction with a certain protein is based on its reactivity and specificity that in turn is determined by reduction potentials and physical properties (e.g., accessibility and electrical charge).

Nonfunctional redox centers in exposed areas of proteins present an interesting target; cystine disulfide residues in particular efficiently compete for reducing CO_2^- radicals to produce disulfide radical anions, a reaction that has been utilized in several cases, yet may also be a problem as it may disfavor designed reactions with functional redox centers. An additional advantage of the PR method over flash photolysis is noteworthy: Usually, the whole spectral range is available for monitoring induced ET reactions, as stated above because the reactive species are solvent derived rather than from a chromophore of the solute. The combination of a wide range of reactivity of the produced reagents with time resolution that extends from nanoseconds to minutes along with convenient spectroscopic monitoring has made the PR technique highly useful in studies of a wide range of chemical and biochemical ET processes.

Finally, the PR method also enables to perform systematic titrations of a given protein by e.g. sequential introduction of reduction equivalents. Adding a series of pulses was found to be of considerable importance in the study of multisite enzymes, where the distribution and rates of ET depend on their degree of reduction (see below).

The potential of pulse radiolysis for studies of biological redox processes was recognized many years ago (14). However, it was initially employed for studies of radiation damage and only later on was it shown to be an effective tool for investigating ET processes to and within proteins. A great advantage in studies of biochemical redox processes is the capability of the PR method to produce the reactive (reducing or oxidizing) species *in situ* and almost instantaneously (i.e., on time scales relevant to those of biological processes). Depending on pH, concentration, and choice of scavengers, the primary aqueous radicals produced by the radiation pulse can be converted into particular inorganic or organic reagents that are appropriate for the reaction to be investigated. Two main interests have guided PR studies of redox proteins: First, elucidation of reaction mechanisms of these proteins, and, second, resolving the parameters that determine the rates of ET within proteins. Obviously, these complement each other. The fast progress attained during the last two decades in resolving 3D structures of a large number of redox active proteins has provided insights that are essential for a meaningful analysis and interpretation of the kinetic results derived from PR studies.

III. COPPER PROTEINS

A. Azurins, a Model System

Azurins are single copper proteins that function as electron mediators in the energy conversion systems of many bacteria (15). While azurins isolated from distinct bacteria are highly homologous, subtle sequence differences do exist,

conferring upon these proteins some variation in reactivity and redox potentials. Azurins have a characteristic β-sandwich structure (16) and contain a single disulfide bridge [Cys3–Cys26] at one end of the molecule separated from the blue (or type1, T1) copper ion by a distance of 2.6 nm (Fig. 1).

CO_2^-radicals reduce azurin either at the Cu(II) site (followed at 625 nm; $\varepsilon = 5,700\,M^{-1}\,\mathrm{cm}^{-1}$) or the disulfide center (followed at 410 nm; $\varepsilon = 10,000\,M^{-1}\,\mathrm{cm}^{-1}$) (Eqs. 13 and 14) with similar, nearly diffusion controlled rates (17). In those molecules where disulfide radicals were formed, they were found to decay by reducing the Cu(II) ion via intramolecular ET (Eq. 15).

$$\mathrm{RSSR{-}Az(Cu^{II})} + \mathrm{CO_2^-} \rightarrow \mathrm{RSSR{-}Az(Cu^{I})} + \mathrm{CO_2} \tag{13}$$

$$\mathrm{RSSR{-}Az(Cu^{II})} + \mathrm{CO_2^-} \rightarrow \mathrm{RSSR^-{-}Az(Cu^{II})} + \mathrm{CO_2} \tag{14}$$

$$\mathrm{RSSR^-} - \mathrm{Az(Cu^{II})} \rightarrow \mathrm{RSSR{-}Az(Cu^{I})} \tag{15}$$

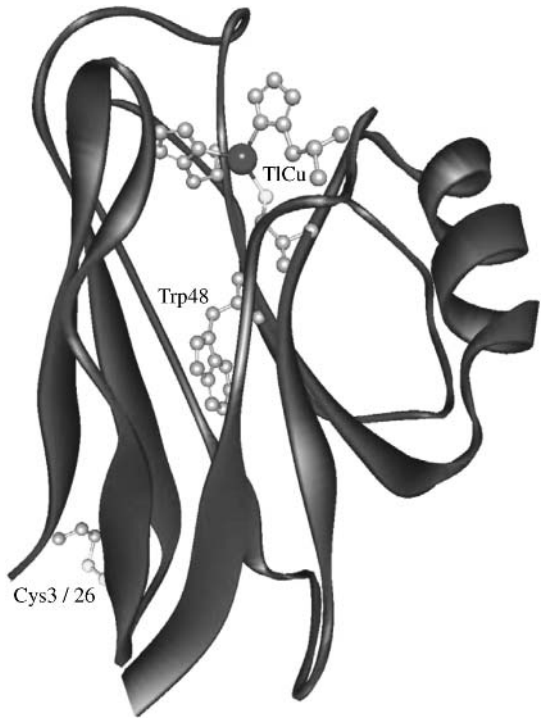

Figure 1. Three-dimensional structure of *Pseudomonas aeruginosa* azurin (16). In addition to the protein backbone, the side chains of three copper ligating residues, His46, His117, and Cys112 are shown near the top together with the disulfide bridge (bottom) and Trp48 (center). Coordinates were taken from the Protein Data Bank (PDB), code 4AZU. (See color insert.)

Examples of time-resolved absorption changes occurring upon reaction of azurin with CO_2^- radicals are illustrated in Fig. 2. Following a fast, direct bimolecular reduction of the two redox active centers at either 625 nm (Eq. 13) or 410 nm (Eq. 14), a slower, concentration independent, unimolecular process takes place

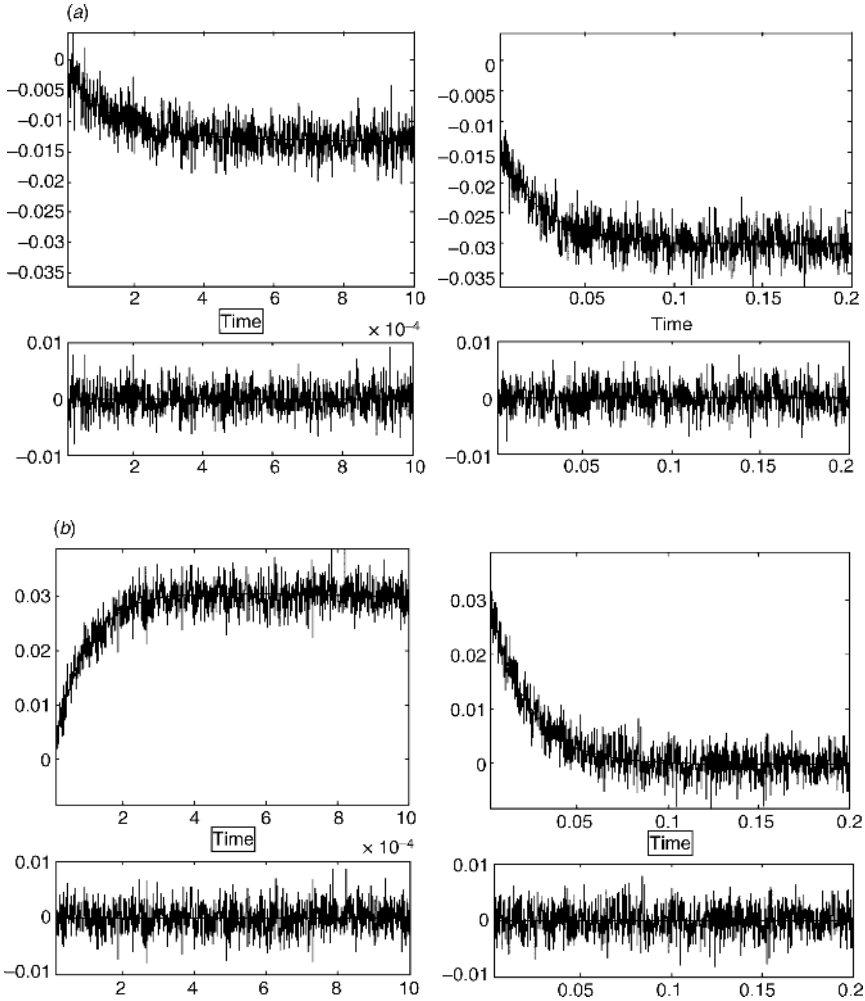

Figure 2. Time-resolved absorption changes induced by reaction of pulse radiolytically produced CO_2^- radicals with *P. aeruginosa* azurin. (*a*) Reduction of Cu(II) followed at 625 nm. (*b*). Formation and decay of the disulfide radical anion measured at 410 nm. Protein concentration is 10μ*M*, where $T = 298$ K; pH 7.0; 0.1 *M* formate; 10 m*M* phosphate; N_2O saturated; pulse width 0.4 μs optical path 12.3 cm. Time is in seconds; the left panel shows the faster phase, while the right one shows the reaction taking place at the slower phase. The lower panels show the residuals of the calculated fits to the data.

attributable to electron transfer from $RSSR^-$ to T1Cu(II) (Eq. 15). For wild-type *P. aeruginosa* azurin the rate of intramolecular ET is $k_{ET} = 44 \pm 7\,s^{-1}$ at pH 7.0 and 25°C at a driving force, $-\Delta G^\circ = 68.9\,kJ\,mol^{-1}$ (17). From temperature-dependence studies of the internal ET reaction the activation enthalpy and activation entropy were determined to be, $\Delta H^{\neq} = 47.5 \pm 4.0\,kJ\,mol^{-1}$; $\Delta S^{\neq} = 56.5 \pm 7.0\,J\,K^{-1}\,mol^{-1}$, respectively. Intramolecular ET between the Cys3/Cys26 disulfide radical anion and the blue Cu(II) center was further studied in a large number of both wild type and single site azurin mutants (17–24). Rates and activation parameters derived from these studies are given in Table I. A linear relationship between activation enthalpy and entropy for a series of homologous reactions is often found (25, 26); and, a plot of the activation enthalpy against the activation entropy for a range of both wild-type and single-site azurin mutants (Fig. 3) is linear with a slope of $T_C = 258 \pm 6\,K$ (and a correlation coefficient of 0.99). Such *enthalpy–entropy compensation* is commonly found for closely related reactions, with observed slopes in the 250–315 K range for reactions in aqueous solution (26, 27). Hypotheses explaining enthalpy–entropy compensation include changes in solvent reorganization, particularly in hydrogen bonding solvents (26, 27). While such linear behavior may indeed be related to the properties of solvent water, deviation of certain data from the linear relationship is usually rationalized by a divergent property of that particular reaction. In the following sections, some of the divergent cases will be addressed. As a consequence of the compensation temperature, T_C, being close to the experimental temperature range, the observed free energy of activation, $\Delta G^{\neq}$, at 298 K is virtually the same ($63 \pm 4\,kJ\,mol^{-1}$) over the full range of azurins investigated, although a small systematic decrease in $\Delta G^{\neq}$ with decreasing $\Delta S^{\neq}$ is observed and is reflected in a small but steady increase in the ET rate.

The possibility of introducing single-site mutations in azurins enabled a detailed analysis of structure–reactivity relationships where, for example, the impact of specific amino acid substitutions on the rate of intramolecular ET could be investigated. In order to understand better the role of the polypeptide matrix separating electron donor and acceptor on ET reactivity, the structure-dependent theoretical model developed by Beratan et al. (6, 7) was employed to identify relevant ET pathways (cf. Section I.B). In this model, the total electronic coupling of a pathway is calculated as a repeated product of the couplings of the individual links. The optimal pathway connecting the two redox sites, $\prod\varepsilon$, is thus identified (cf. Eq. 5).

Pathway calculations for the aforementioned intramolecular ET reaction were performed using the high-resolution 3D structures of *P. aeruginosa* azurin and its mutants, where available. For other mutants, structures based on two-dimensional nuclear magnetic resonance (2D NMR) studies and energy minimization calculations were employed. The pathway calculations predict similar ET routes in all the azurins shown in Fig. 4: One longer path through the peptide

TABLE I
Kinetic and Thermodynamic Data for the Intramolecular reduction of Cu(II) by $RSSR^-$ in AZURIN; pH 7.0

Azurin	k_{298} (s^{-1})	E' (mV)	$-\Delta G^\circ$ (kJ mol^{-1})	$\Delta H^{\neq}$ (kJ mol^{-1})	$\Delta S^{\neq}$ (JK^- mol^{-1})
Wild Type					
P. aeruginosa[a]	44 ± 7	304	68.9	47.5 ± 2.2	-56.5 ± 3.5
P. fluorescense[b]	22 ± 3	347	73.0	36.3 ± 1.2	-97.7 ± 5.0
Alc. spp.[a]	28 ± 1.5	260	64.6	16.7 ± 1.5	-171 ± 18
Alcalegenes faecalis[b]	11 ± 2	266	65.2	54.5 ± 1.4	-43.9 ± 9.5
Alc. denitrificans	42 ± 4	305	69.0	43.5 ± 2.5	-67 ± 9
Mutant					
D23A[c]	15 ± 3	311	69.6	47.8 ± 1.4	-61.4 ± 6.3
F110S[d]	38 ± 10	314	69.9	55.5 ± 5.0	-28.7 ± 4.5
F114A[e]	72 ± 14	358	74.1	52.1 ± 1.3	-36.1 ± 8.2
H35G.aq[f]	15 ± 2	<300	<68.5	42.1 ± 3.5	-81 ± 5
H35Q[g]	53 ± 11	268	65.4	37.3 ± 1.3	-86.5 ± 5.8
H117G.aq[g]	7 ± 3	<300	<68.5	22.0 ± 3.2	-155 ± 11
H117G.im[h]	149 ± 17	240 ± 20	62.7	54.5 ± 3.9	-22 ± 1
17S[d]	42 ± 8	301	68.6	56.6 ± 4.1	-21.5 ± 4.2
M44K[g]	134 ± 12	370	75.3	47.2 ± 0.7	-46.4 ± 4.4
M64E[d]	55 ± 8	278	66.4	46.3 ± 6.2	-56.2 ± 7.2
M121H[f]	21 ± 47	215	60.3	28.0 ± 2.1	-127 ± 8
M121L[d]	38 ± 7	412	79.3	45.2 ± 1.3	-61.5 ± 7.2
V31W[h]	285 ± 18	301	68.6	47.2 ± 2.4	-39.7 ± 2.5
W48F[h]	35 ± 7	301	68.6	46.3 ± 5.9	-58.3 ± 6.0
W48F[h]	80 ± 5	304	68.9	43.7 ± 6.7	-61.9 ± 9.7
W48[h]	50 ± 5	314	69.9	49.8 ± 4.9	-44.0 ± 3.5
W48Y[h]	85 ± 5	323	70.7	52.6 ± 6.9	-30.2 ± 3.6
W48L[e]	40 ± 4	323	70.7	48.3 ± 0.9	-51.5 ± 5.7
W48M[e]	33 ± 5	312	69.7	48.4 ± 1.3	-50.9 ± 7.4

[a]Ref. (17).
[b]Ref. (18).
[c]Ref. (21).
[d]Ref. (22).
[e]Ref. (19).
[f]Ref. (24).
[g]Ref. (20).
[h]Ref. (23).

chain to the copper-ligating imidazole of His46, and one shorter path through the buried indole ring of Trp48, necessitating a through-space jump to this residue. The electronic coupling factors were found to be 2.5×10^{-7} and 3.0×10^{-8}, respectively. However, in this analysis, the electronic interaction between the Cu(II) ion and its ligands was not included. It has been demonstrated

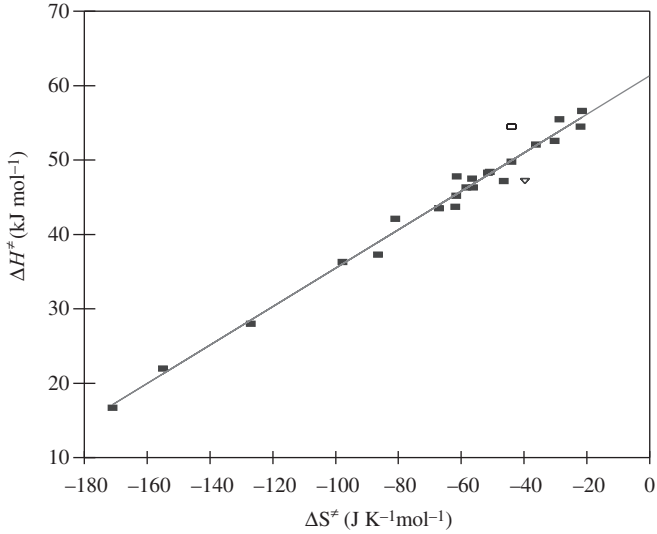

Figure 3. Activation enthalpy–activation entropy compensation plot. Activation enthalpy values determined at 298 K plotted as a function of activation entropy. The straight line is the result of a linear least-squares fit to all data points and has a slope of 258 ± 6 K (24). Two points, representing WT *A. faecalis* azurin (□) and the V31W mutant (▽), respectively, are discussed in the text.

that the high degree of anisotropic covalency in the copper coordination site would enhance ET through the Cys112 thiolate ligand (28). By similar arguments, from the ligand coefficients of Ψ_{HOMO} (HOMO = highest occupied molecular orbital) in azurin calculated by Larsson et al. (29), it can be estimated that ET through the Cys thiolate would be enhanced by a factor of ~150 over ET via one of the His imidazole ligands. The pathway calculations combined with the notion of anisotropic covalency would therefore suggest that the ''Trp48'' pathway would offer better coupling than one going through His46. Since the same LRET pathway from $RSSR^-$ to Cu(II) applies to all azurins studied so far, it was possible, from the kinetic data and activation parameters to calculate the reorganization energy, $\lambda_{tot} = 1.0 \pm 0.05$ eV, and the experimental decay factor, $\beta = 10.0 \pm 0.5\,nm^{-1}$ (22).

In order to probe the possible influence of aromatic residues on internal ET, an investigation was initiated on single-site azurin mutants in which Trp48 had been substituted by other amino acids, with both aromatic and nonaromatic side chains. In the experiments, the rate constants for intramolecular ET were determined as a function of temperature (23). The results are set out in Table I together with the standard free energies of reaction (ΔG°), the activation enthalpy ($\Delta H^{\neq}$) and activation entropy ($\Delta S^{\neq}$). It is clear that substitution of

Trp48 by other amino acids only has a small effect on the kinetic parameters after correcting for changes in driving force.

In further studies of this aspect, another mutant was constructed in which Val31 was substituted by Trp, thus producing a double-Trp mutant (V31W azurin) where the two indole rings are placed in neighboring positions (23). The spatial relationship between the two indole rings, in the V31W mutant, was investigated by two-dimensional nuclear overhauser enhancement spectroscopy (2D NOESY) and total correlated spectroscopy (TOCSY) experiments. Two spin systems consisting of four peaks (tryptophans) could immediately be identified from the TOCSY spectra; these systems were assigned to residues 31 and 48 (23). A large number of residues exhibited chemical shift values identical with those of the corresponding residue in the wild-type protein (30). The chemical shifts of the four protons of the Trp48 side chain are within 0.1 ppm of those of the wild-type protein, indicating similar orientation. Thus, the side chain of Trp31 is probably positioned above the plane of the Trp48 indole, since the signals of the Trp31 side chain are upshifted. Both tryptophans have nuclear overhauser effects (NOEs) between their side chains and methyl groups of an isoleucine and a valine, probably Ile7 and Val95. These NOEs put further constraints on the orientation of the Trp31 side chain. The two ring systems are not stacked in a parallel fashion, but they form an oblique angle relative to each other. Thus, the NMR data show that the regions in the mutant located behind Trp 48 (relative to Trp31) have the same structure as the equivalent regions in the wild-type (WT) protein. Energy minimization calculations have also been performed on this mutant and show a close (van der Waals) contact of the two indole rings consistent with the observation of NOEs between the ring protons (23).

The $RSSR^-$ to Cu(II) LRET in the V31W azurin mutant was found to take place with a rate constant of $285\,s^{-1}$ (298 K, pH 7.0, and similar driving force as in WT azurin), which is a considerably faster reaction than for any other azurin studied so far (cf. Table I). The high rate strongly suggests that the main ET route is the Trp48 pathway, since the one through His46 should not be affected directly by this mutation. The activation enthalpy and entropy of this LRET were also examined. The dependence of the activation enthalpy on reorganization energy is given by Eq.6. In azurins, where Trp48 has been exchanged by other amino acid residues, $\Delta H^{\neq}$ is constant within experimental error, consistent with the previous assumption that the reorganization energies do not change significantly in this series.

The entropy of activation, which includes a contribution from the separation distance dependence of the electronic coupling is given by Eq.7. It is seen that the increase in rate in V31W azurin follows from a more favorable entropy of activation (Table I), which is larger by $16.8\,J\,K^{-1}mol^{-1}$ compared with WT azurin. Since ΔS° can safely be assumed to be the same for intramolecular ET in

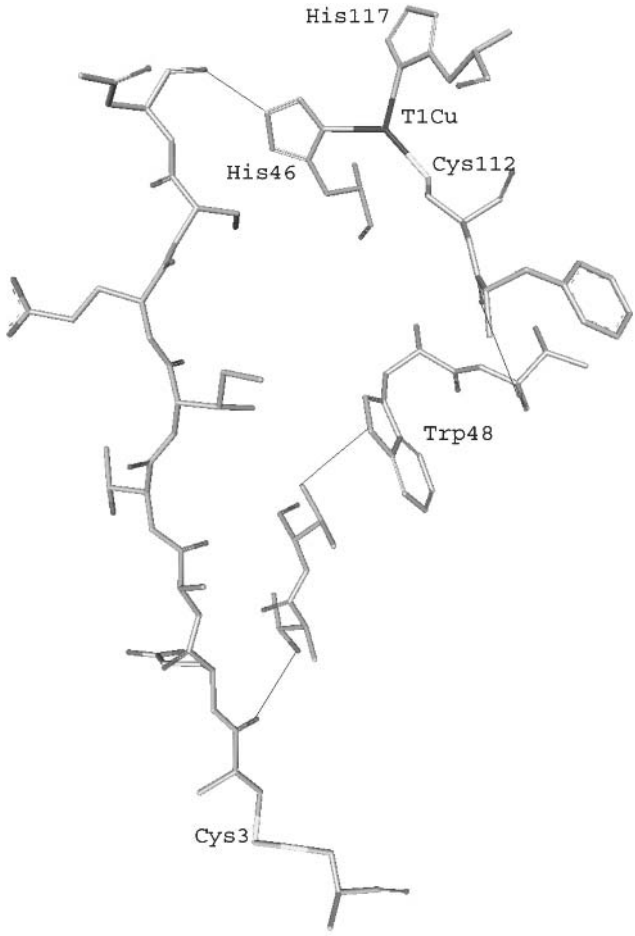

Figure 4. Calculated ET pathways in *P. aeruginosa* azurin from the sulfur atom of Cys3 to the copper ligands His46 and Cys112 applying the Beratan and Onuchic model (6, 7). The left path consists of 27 covalent bonds and one hydrogen bond, while the right pathway includes 21 covalent bonds, two hydrogen bonds, and one van der Waals contact. Noncovalent connections are also shown. Coordinates were taken from the PDB, code 4AZU.

WT and V31W azurins, the increase in entropy would according to Eq.7 correspond to a decrease in $\beta(r - r_0)$ from the previously determined value of 24.6 in WT to 22.6 in V31W azurin. A smaller exponential decay factor, β, for the mutant is also reflected in the electronic coupling matrix element, H_{DA}, between electron donor and acceptor, which was found to be 2.1×10^{-7} eV (23), or an improvement of a factor 2.6 relative to WT azurin ($H_{DA} = 0.8 \times 10^{-7}$ eV). In contrast, a calculation of the electronic coupling

factor that treats all covalent bonds equally yielded $\Pi\varepsilon = 0.9 \times 10^{-8}$ for V31W azurin as compared with 3.0×10^{-8} for WT azurin (19). The relative positions of Trp31 and Trp48 in Val31Trp azurin may enhance the interaction between D and A, since the aromatic ring systems are in van der Waals contact; this close contact (with a large electronic overlap) may give rise to resonance-type tunneling through the two indole rings. Aromatic residues placed in appropriate positions may enhance ET through proteins by providing more effective coupling through their extended π^* orbitals, since the energy gap between the tunneling electron and the aromatic π system is significantly smaller than that involving σ orbitals. A single aromatic residue placed midway between D and A in a predominantly σ-ET pathway is not advantageous by itself, however, since $\sigma \rightarrow \pi \rightarrow \sigma$ ET will be energetically unfavorable.

However, several aromatic residues placed in successive positions or aromatic molecules in direct contact with either D or A would act as an extended relay that could enhance the electronic coupling (24).

The relevance of the Trp48 route is further confirmed by the pronounced deviation of two data sets from the linear relationship between the activation entropy and enthalpy (cf. Fig. 3), namely for WT *A. faelcalis* azurin (□) and for the *P. aeruginosa* Val31Trp azurin mutant (▽). The WT azurin from *A. f.* is unique among azurins since it has Val at position 48 (instead of a Trp). The absence of the aromatic residue here is noteworthy, since Fig. 3 demonstrates that the point for this particular azurin clearly falls above the line (an unusually slow ET rate), whereas the point for the V31W mutant with two stacked aromatic residues falls below the line (reflecting the fast ET rate).

Aromatic residues have been found in proteins at positions that probably enhance the electronic coupling in systems that have been selected by evolution for efficient ET. Examples are the tryptophan mediated reduction of quinone in the photosynthetic reaction center (31), the methylamine dehydrogenase (MADH): amicyanin system, where a Trp residue is placed at the interface between the two proteins (32), as well as the [cytochrome *c* peroxidase–cytochrome *c*] complex, where a Trp seems to have a similar function (33).

In order to further distinguish between the possible pathways for ET in azurins, several azurin mutants were produced where two of the copper ligating amino acids, His46 and His117, were systematically replaced by a noncoordinating glycine, while the third T1 ligand, Met121, was replaced by a histidine (24). Of course these modifications of the copper-binding site also change other properties of the site (e.g., its redox potential and the charge distribution on the metal ion). An influence of electron delocalization on the electronic coupling between donor and acceptor will appear as an apparent change in the activation entropy (cf. Eq. 7). Indeed, a decrease in electron density on the cysteine was evident in the observed larger EPR hyperfine splitting (A_z) of the different mutants, Met121His, His46Gly, and His117Gly (34).

The relevance of the His46 pathway relative to the Trp48 route was investigated in experiments using the aforementioned mutants, where the His ligands had been replaced by glycine (24). The former pathway would be blocked when the linkage to the copper ion via the hydrogen bond from Asn10 to His46 is lost (cf. Fig. 3). However, this mutation does considerably modify the coordination sphere of the copper ion (35), a change that could affect the ET rate. Therefore, in order to investigate the influence of the change in the electronic properties caused by removal of a His ligand and its effect on the ET rate, the kinetics of ET in a similar mutant, *P. aeruginosa* His117Gly azurin, were also studied (24). The His117 provides the other imidazole residue coordinated to the copper ion in azurin. The Cu(II) ion in both *P. aeruginosa* His46Gly and *P. aeruginosa* His117Gly mutants was found to be accessible to external ligands, which upon coordination to the metal ion, obviously perturb its spectroscopic features (35–37).

When imidazole (im) is added in sufficient concentration to coordinate the copper ion in *P. aeruginosa* azurin mutants His46Gly or His117Gly, the green mutants turn blue with absorption bands at 628 nm (His117Gly·im) and 621 nm (His46Gly·im), which are close to that of WT-azurin (626 nm) (35, 36). Other spectroscopic features, including those from EPR, electron–nuclear double resonance (ENDOR), and resonance Raman measurements, are restored, implying that the structures of the mutants, specifically metal-binding site geometries, are maintained despite the replacement of histidine by imidazole.

Intramolecular ET in His117Gly·im azurin is considerably faster than in WT *P. aeruginosa* azurin in spite of the lower driving force (Table I). Since their activation enthalpies are the same within experimental error, the reorganization energy is probably not changed significantly (cf. Eq. 6). In spite of the large difference in ET rates (cf. Table I), the points for His117Gly·aq, His46Gly·aq, His117Gly·im, and WT *P.a.* azurin fit perfectly on the free energy ($\Delta H^{\neq}$ vs. $\Delta S^{\neq}$ compensation) plot shown in Fig. 3. In His46Gly·aq and His117Gly·aq, water molecules can enter the copper coordination sphere and give rise to rather large changes in the solvation sphere. Inserting an imidazole, however, which is perfectly accommodated in the pocket of H117G azurin, will prevent water from approaching the redox site. Nevertheless, all three data points extending over the full range of the plot (Fig. 3) lie on the straight line as expected, consistent with the operation of one and the same ET mechanism, thereby providing further support for the Trp48 ET pathway from the disulfide radical to Cu(II).

A strong pH dependence is observed for the rate constant of the intramolecular $RSSR^{-} \rightarrow$ Cu(II) LRET in all the different wild-type and single-site azurin mutants studied so far, with the rate constant increasing by an order of magnitude upon decreasing the pH from 8 to 4 (21). In order to rationalize the influence of pH on ET reactivity, the different parameters that determine the LRET rates were considered: Driving force, reorganization energy, distance

between electron donor and acceptor, and the nature of the protein medium separating the redox couple.

The reduction potential of *P. aeruginosa* azurin increases by 60–70 mV upon changing pH from 10 to 5 (38–40). The NMR studies addressed the question of how much protonation of the two conserved titratable histidines in azurin, His35 and His83, may increase the Cu(II)/Cu(I). It was found that the contributions from these two residues are 50 and 13 mV, respectively (40). There is a problem here, however, since the reduction potential of the H35K azurin mutant displays essentially the same pH dependence as WT (39), which seems to speak against this hypothesis, unless the protonated lysyl ε-amine group has an unusually low pK value.

All other wild-type and mutated azurins studied so far exhibit a similar change of ~60 mV in reduction potential upon going from neutral solutions to lower pH (38–40). For the WT *P. aeruginosa* azurin, this would correspond to an increase in driving force ($-\Delta G^\circ$) from 68.9 to 74.7 kJ mol^{-1}. Equation 2 predicts an increase in intramolecular ET rate constant from 44 to 61 s^{-1}, which is far less than observed experimentally ($k = 285\,\mathrm{s}^{-1}$ at pH 4.0 and 25°C) (21). Moreover, the same pH dependence is also observed for LRET in H35Q azurin, where no protonation of residue 35 is possible (20); this would exclude any effect of His35 protonation on either reduction potential or intramolecular ET kinetics. Another candidate for modifying the LRET driving force is Asp23. According to the 3D structure of *P. aeruginosa* azurin (16), this residue is proximal to the electron donor, the $RSSR^-$ radical, with its peptide carbonyl hydrogen bonded to the amide N of Cys26 and with one of its carboxyl oxygens within hydrogen-bond distance to two neighboring residues that could increase the pK of Asp23 from the regular value to 6.2. However, any key role of this residue can now also be excluded, since the same LRET pH dependence is observed for the D23A mutant as with all the other azurins studied so far. Finally, the $RSSR^-$ radical anion has a pK of ~6 (41), but protonation is expected to lower the reduction potential, owing to the elimination of electrostatic charge, and thus we tend also to exclude this residue as a cause of the rate acceleration.

Most importantly, as shown in the following, it is impossible to reconcile any increase in driving force with the observed pH dependence of the rate for WT azurin; with $\lambda = 1.0$ eV, $\beta(r - r_0) = 24.6$, and $-\Delta G^\circ = 0.71$ eV, Eq. 2 gives a maximum rate constant, $k_{max} = 210\,\mathrm{s}^{-1}$, which is still smaller than the experimentally observed value at low pH, $285\,\mathrm{s}^{-1}$. Further increase in the driving force above the value of the reorganization energy would only bring the system into the inverted region where the rate constant will decrease again (cf. Eq. 2). For the same reason, a rate acceleration caused by changes in reorganization energy, λ, due to protonation of a specific protein site can be excluded. It should also be emphasized that the rate increase at low pH is due to an entropy effect rather than to a more favorable enthalpy term. The exponential term in Eq. 3 is also

included in the calculated entropy of activation (cf. Eq. 7). Hence, the rate increase logically is the result of slightly better electronic coupling between electron donor and acceptor. Indeed, the increase in specific rate of LRET in WT *P. aeruginosa* azurin from 44 to 285 s^{-1} can be accounted for by reducing the exponential term, $\beta(r - r_0)$ from 24.6 calculated for WT azurin at pH 7 (22) to 23.6. Careful examination of the 3D structures of azurin determined at both pH 5.5 and 9.0 (16) shows no structural changes in the region of the calculated electron tunneling pathways. The only major conformational change observed involves a Pro36–Gly37 main chain peptide bond flip, and these residues are not involved in the pathways. Still, a decrease in ET distance of 0.3 nm would be sufficient for rationalizing the rate increase observed at low pH. An alternative explanation would be a slight decrease in the distance decay factor, β, from 10.0 to 9.6 m^{-1}. Obviously, more experimental work is required combined with a more detailed examination of possible hydrogen bonds present in azurin, in order to unequivocally identify the cause(s) for the observed marked pH induced acceleration of the LRET rate constant.

In order to gain further insight into the possible impact of the solvent on LRET in *P. aeruginosa*. azurin, rates of intramolecular ET in water have been compared with those in deuterium oxide (42). Unexpectedly, the kinetic isotope effect, k_H/k_D, was found to be *smaller* than unity (0.7 at 298 K), primarily as a result of differences in activation entropies in H_2O ($-56.5\,J\,K^{-1}\,mol^{-1}$) and in D_2O ($-35.7\,J\,K^{-1}\,mol^{-1}$), which in turn suggests a distinct role for protein solvation in the two media. This notion is further supported by results of voltammetric measurements where the reduction potential of Cu(II)/Cu(I) was found to be 10 mV more positive in D_2O at 298 K. The standard entropy changes also differ ($-57\,J\,K^{-1}\,mol^{-1}$ in water and $-84\,J\,K^{-1}\,mol^{-1}$ in deuterium oxide) (42) and thus make different contributions to the activation entropies (cf. Eq. 8). Isotope effects are also inherent in the nuclear term of the Gibbs free energy, as well as in the tunneling factor. A slightly larger thermal protein expansion in H_2O than in D_2O (0.001 nm K^{-1}) is sufficient to account for both activation and standard entropy differences. Thus, differences in driving force and thermal expansion seem to be the simplest rationales for the observed isotope effect (42). These observations once more underscore the important role of solvent in affecting the rates of internal ET in proteins.

A very different approach to studies of internal ET in azurin employed an Asn42Cys mutant which under oxidizing conditions forms a dimer where the two azurin monomers are covalently linked via the Cys42–Cys42 disulfide bridge (43). The 3D structure of the dimer has been determined and the short intermolecular disulfide link was found to cause a strong steric constraint (44). This new type of engineered azurin was employed in order to investigate ET between the pulse radiolytically produced disulfide radical ion and Cu(II) over a considerably shorter distance than in the monomer (1.28 nm for Cys42 to Cu in

the dimer as compared with 2.59 nm for Cys3–Cys26 to Cu in the previous studies). In order to avoid possible interference from reduction of the native Cys3–Cys26 disulfide bond, a triply mutated azurin was constructed and expressed, where the latter two cysteines were substituted by alanines, Cys3Ala–Cys26Ala–Asn42Cys. Earlier structural studies of an azurin mutant, where this disulfide bridge has been eliminated (Cys3Ala–Cys26Ala) established that the overall structure of the protein is not changed and the only difference is in the immediate proximity of the mutated residues (45).

Reacting the azurin dimer with pulse radiolytically produced CO_2^- radical anions, the intermolecular disulfide bridge becomes reduced forming the $RSSR^-$ radical in an essentially diffusion controlled reaction ($k_1 \simeq 10^9\, M^{-1}\, s^{-1}$). In contrast to the behavior of monomeric azurins, no competing bimolecular reduction of the blue Cu(II) center by CO_2^- was observed. Disulfide reduction was followed by concentration independent, intramolecular $RSSR^- \rightarrow Cu^{(II)}$ ET (Fig. 5):

$$RSSR^- - Az(Cu^{II}) \xrightarrow{k_2} RSSR - Az(Cu^{I}) \qquad (16)$$

The process was studied at pH 7.0 over a dimer concentration range from 5 to 54 μM and monitored at both 410 nm ($RSSR^-$ absorption, $\varepsilon_{410} = 10,000\ M^{-1}\, cm^{-1}$) and at 625 nm [Cu(II) absorption, $\varepsilon_{625} = 5,000\, M^{-1}\, cm^{-1}$) (43).

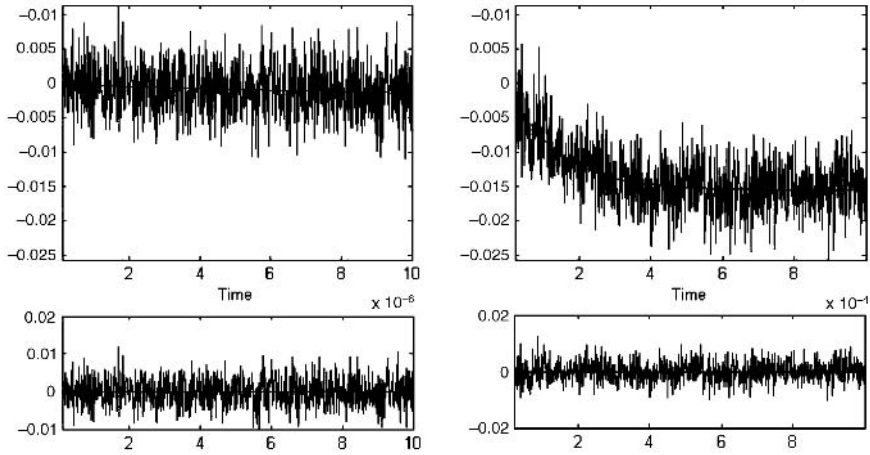

Figure 5. Time-resolved absorption changes, induced by reaction of CO_2^- radicals, due to intramolecular ET from the internal disulfide radical anion to Cu(II) in the C3/C26A–N42C azurin dimer measured at 625 nm. Protein concentration was 20μM, where $T = 299$ K; pH 7.0; 0.1 M formate; 10 mM phosphate; N_2O saturated; pulse width 1.5 μs; optical path 3 cm. Time is in seconds; the left panel shows the faster phase, while the right one shows the reaction taking place at the slower phase. The lower panels show residuals of the fits to the data.

The intramolecular ET rate constant, k_2, was found to be $7200 \pm 100\,s^{-1}$ at 25°C and pH 7.0 (43). The employed protocol exposed each solution to only few pulses causing $< 10\%$ reduction of the molecules present. Hence, the probability of reducing more than one of the Cu(II) ions in a dimer is negligible. From the temperature dependence of the internal ET rate (studied from 3.2 to 40.0°C) the activation parameters were derived (Table II). Finally, results of intramolecular ET measurements in the triply mutated azurin dimer showed that its rate constant is in good agreement with the Beratan and Onuchic (6) tunneling pathway model. The polypeptide chain in the azurin dimer links S_γ of Cys42 with N_δ of His46, which provides one of the copper ligands (Fig. 6). This pathway consists of 17 covalent bonds and the distance between the copper ion and the sulfur atom of the same monomer is 1.29 nm. Driving force optimized rate constants for ET in a β-sheet protein can be described by an average coupling decay constant of $10.0\,nm^{-1}$ (46), which leads to an activationless $k_{max} = 10^5\,s^{-1}$ (i.e., when the driving force, $-\Delta G^\circ$ equals the reorganization energy, λ). Assuming that the previously determined reorganization energy and driving force for intramolecular ET between the Cys3–Cys26 $RSSR^-$ and the copper center in WT *P. aeruginosa* azurin ($\lambda_{tot} = 1.0\,eV$ and $-\Delta G^\circ = 0.71\,eV$) (22) are also applicable to the present mutant dimer, a rate constant of $4 \times 10^4\,s^{-1}$ at 298 K is calculated that is still fivefold larger than the experimentally observed rate, $k_{298} = 7200\,s^{-1}$. Though not an unreasonably large discrepancy, a rationale may be considered for the divergence: In native *P. aeruginosa* azurin the ET pathway includes S_λ of Cys112, while tunneling from the external C42/C42 disulfide bridge to the copper center proceeds via the N_δ of His46. It has already been pointed out that there is a high degree of anisotropic covalency in the blue Cu(II) center (28, 29): While 50% of the electron density is concentrated on the Cu–sulfur bond only 4% is found on

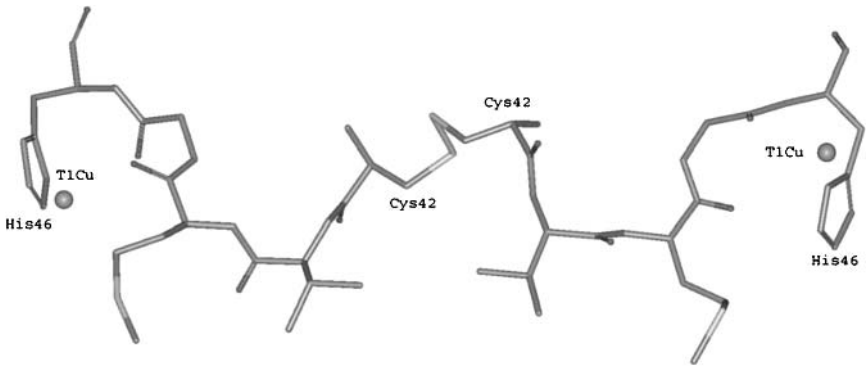

Figure 6. Electron-transfer pathway in the azurin dimer mutant (43). The path connects S_γ of Cys42 with N_δ of His46, which is one of the copper ligands, and consists of 17 covalent bonds resulting in a very effective electronic coupling of the two redox centers. Calculations were based on the Beratan and Onuchic model (6, 7). Coordinates were taken from the PDB, code 1JVO.

each of the ligating imidazoles, which would drastically diminish the electronic coupling in the dimer compared with the former one and cause the observed lower rate.

An additional interesting observation emerged from a comparison of the activation parameters calculated here for the azurin dimer with those obtained earlier for azurins as well as for related blue copper containing enzymes (cf. later sections): In all (single copper) azurins, the $RSSR^-$ to copper(II) LRET is controlled by a relatively large activation enthalpy, while in multicopper proteins, including the present azurin dimer as well as systems like cytochrome *c* oxidases, the activation enthalpies are relatively small and the large negative activation entropies were found to be rate determining, although in these proteins the connecting ET pathways are considerably shorter. One rationale could be that major solvent reorganization takes place in all monomeric azurins upon ET where the intramolecular Cys3–Cys26 disulfide bridge is considerably more solvent exposed than is the intermolecular Cys42–Cys42 cystine of the dimer. This hypothesis is corroborated by the observed excellent linear correlation between the activation enthalpy and entropy data presented in Table II that point to an overriding influence of solvent effects.

Finally, the ET reactivity of the binuclear Cu_A site present in cytochrome *c* oxidase and nitrous oxide reductase illustrates an additional interesting

TABLE II
Rate Constants and Activation Parameters for Internal ET in Different Copper-Containing Proteins

Protein	ET Process	k_{298} (s^{-1})	$\Delta H^{\neq}$ (kJ mol^{-1})	$\Delta S^{\neq}$ (J $K^{-1}mol^{-1}$)	ET Distance (nm)
P. aeruginosa azurin[a]	$RSSR^- \rightarrow Cu^{2+}$	44 ± 7	47.5 ± 4	-56.5 ± 7.0	2.56
C3/26A-N42C dimer[b]	$RSSR^- \rightarrow Cu^{2+}$	7200 ± 100	17.7 ± 2.0	-112 ± 6	1.28
CuNiR[c]	$T1Cu^I \rightarrow T2Cu^{II}$	185 ± 12	22.7 ± 3.4	-126 ± 11	1.27
Ascorbate oxidase[d]	$T1Cu^I \rightarrow T2/T3Cu^{II}$	201 ± 8	9.1 ± 1.1	-170 ± 9	1.22
Cytchrome *c* oxidase (bovine)[e]	$Cu_A{}^I \rightarrow$ heme-c^{III}	$13{,}000 \pm 1{,}200$	11.4 ± 0.9	-128 ± 11	1.96
Cytchrome *c* oxidase (bacterial)[f]	$Cu_A{}^I \rightarrow$ heme-c^{III}	$20{,}400 \pm 1{,}500$	22.2 ± 1.2	-88 ± 2	1.96

[a]Ref. 17.
[b]Ref. 43.
[c]Ref. 47.
[d]Ref. 48.
[e]Ref. 49.
[f]Ref. 50.

application of PR in azurin. The Cu_A serves as the electron uptake center in the above enzymes, and its discovery raised a considerable debate regarding the causes for the evolution of multiple forms of copper electron mediation centers (i.e., T1 and Cu_A). An azurin mutant, the so-called ''purple'' azurin, has been engineered by Lu and co-workers (51). In this mutant, the amino acids forming the blue type 1 (T1) copper site have been replaced by residues constituting the Cu_A site of *Paracoccus denitrificans* cytochrome *c* oxidase. The close overall structural similarity between the native blue copper azurin and the engineered purple Cu_A azurin has been demonstrated by X-ray crystallography (51). Since the T1 and the Cu_A centers are placed in the same location in azurin, while all other structural elements remain the same, the purple mutant is an optimal system for examining the unique electron mediation properties of the binuclear Cu_A center. Analysis of the ET path from the disulfide radical anion to Cu_A shows that the same number of covalent bonds, the same two hydrogen bonds, and the through-space jump are all also found in the purple Cu_A azurin structure. Therefore, the same pathway is most likely operative in the purple azurin. The rate constant of the intramolecular process, $k_{ET} = 650 \pm 60\,s^{-1}$ at 298 K and pH 5.1 (52), is almost threefold faster than for the same process in the wild-type single blue copper azurin from *P. aeruginosa* ($250 \pm 20 s^{-1}$ at this pH), in spite of a smaller driving force (0.69 eV for purple Cu_A azurin vs. 0.77 eV for the blue copper center). Apparently, the presence of a binuclear Cu_A center as the primary electron uptake site in cytochrome *c* oxidase, the terminal enzyme of the respiratory system, rather than the more prevalent T1 copper site, constitutes an illustration of evolutionary selection of a structure better suited for specific requirements of the biological function.

Di Bilio et al. (53) analyzed the intramolecular LRET in Ru(II) modified *P. aeruginosa* azurin and calculated the reorganization energies of both electron donor and acceptor centers from the temperature dependence of the observed rate constants. For the blue, T1 copper center $\lambda_{T1} = 0.82$ eV was reported. Now, from the observed rate of intramolecular ET in purple azurin, $\lambda_{CuA} = 0.4$ eV was calculated for the Cu_A center (52) (i.e., only 50% of the reorganization energy required for the blue copper site, supporting the notion that Cu_A is indeed a redox center with improved ET properties). In conclusion, the purple Cu_A center transfers electrons more efficiently than the blue copper center. This is mainly a result of the low reorganization energy of the mixed-valence [Cu(1.5)–Cu(1.5)] site.

Summarizing the results of studies of intramolecular ET in azurins, it is important to stress that in all probability, the induced ET between the disulfide radical and the blue copper(II) center is not part of any physiological function, and the role of the disulfide is structural, solely. Still, azurin has turned out to be a very useful model system for examination of different parameters controlling LRET rates in proteins. The impact of specific structural changes introduced by single-site mutations has been studied in order to obtain a better understanding

of these parameters, namely, driving force, reorganization energy, as well as distance and structure of the medium separating the redox centers. The ET reactions are well described within the framework of Marcus theory (3), and the electronic coupling model developed by Beratan and Onuchic (6) works well for ET pathway determination. Experience obtained through studies of ET in azurins has been exploited in further studies on multicentered metalloenzymes, which is the subject of the following sections.

B. Copper-Containing Oxidases and Reductases

Intramolecular ET between distinct copper centers is part of the catalytic cycles of many copper-containing redox enzymes, such as the multicopper oxidases, ascorbate oxidase, and ceruloplasmin, as well as the copper-containing nitrite reductases. Examination of internal LRET in these proteins is of considerable interest as it may also provide insights into the evolution of selected ET pathways; in particular, whether and how the enzymes have evolved in order to optimize catalytic functions. With the increase in the number of known high-resolution 3D structures of transition metal containing redox enzymes, studies of structure–reactivity relationships have become feasible and indeed many have been carried out during the last two decades.

The blue multicopper oxidases catalyze the four-electron reduction of dioxygen to water by four sequential one-electron oxidations of their respective substrates (54). These enzymes are widely distributed in Nature, from bacteria, fungi, and plants to mammals. All contain at least four copper ions bound to sites of the following types: (a) The blue type 1 site (T1), also found in azurin (Section III.A), characterized by an intense charge-transfer band in the 600-nm region ($\varepsilon \sim 5,000\,M^{-1}\,cm^{-1}$) and a narrow hyperfine coupling constant ($A_{\|} < 10^{-3}\,cm^{-1}$) extracted from EPR spectra (2). (b) A type 2 (T2) copper center (lacking intense absorption bands) with a *normal* EPR spectrum. (c) A copper ion pair, called type 3 (T3), which in the oxidized state is characterized by an intense absorption in the near ultraviolet (UV) region ($\varepsilon \sim 4,000\,M^{-1}\,cm^{-1}$) and by strong antiferromagnetic coupling. The 3D structural studies have shown that T2 and T3 are proximal and together form a trinuclear cluster (2). The physiological function of T1 is sequential uptake and delivery of single electrons from substrate molecules to the trinuclear center where dioxygen binds is reduced to water. Thus, the enzymatic cycle of the oxidases feature a ping–pong mechanism:

$$2AH_2 + O_2 \xrightarrow{\text{oxidase}} 2A + 2H_2O \tag{17}$$

Intramolecular ET between T1 and the trinuclear T2/T3 center is therefore expected to play a crucial role in the molecular mechanism of this class of

enzymes. High-resolution 3D-crystal structures are now available for ascorbate oxidase (55–58), human ceruloplasmin (59), and its yeast homolog, Fet3p (60), as well as fungal laccase (61). These structures have proven to be very helpful in analysis and interpretation of kinetic results.

Pulse radiolysis was applied to studying ET within multicentred blue oxidases three decades ago (62). However, at that early time, without knowledge of the 3D structures of any of the multicopper proteins, only general conclusions about possible intramolecular ET processes could be made. The PR studies of human ceruloplasmin, hCp, showed that first a diffusion controlled reaction of the enzyme with hydrated electrons takes place, forming transient optical absorptions that are primarily due to surface exposed disulfide radicals. The radicals were found to decay concomitantly with the reduction of the solvent less-accessible T1Cu(II) site by intramolecular ET (62). Thus, even at that stage some insights were gained that were greatly extended later using structural information as it became available.

1. Ascorbate Oxidase

The earliest high-resolution 3D structure of a copper oxidase was reported in 1989, namely, for ascorbate oxidase from *Cucurbita pepo medullosa* (AO cf. Fig. 7), first in a fully oxidized state and eventually also in the reduced state as well as with different exogenous ligands (55–58). Ascorbate oxidase is a 140-kDa dimer, consisting of two identical subunits; each monomer includes three domains with the T1 copper site residing within one domain, while three copper ions form a trinuclear center, consisting of both T2 and T3 in a structural arrangement formed by four histidine imidazoles from one domain and four from another: Of the three copper ions, two are coordinated to six histidines whose nitrogen atoms (five N_ε and one N_δ atom) are arranged in a trigonal prism, reminiscent of the hemocyanin copper site structure, and were, by analogy, called T3 The remaining copper ion, coordinated to two histidines, would then be a T2 site. Importantly, none of the imidazoles is involved in bridging copper ions. The two copper ions constituting the T3 site are bridged by an oxygen atom (either as OH^- or O^{2-}) and at the T2 site a hydroxide ion or water molecule is coordinated to the copper ion. The trinuclear site is accessible to exogenous ligands and may bind anions such as F^-, N_3^-, and CN^- (55–58).

Like all other blue copper oxidases, AO catalyzes the four-electron reduction of dioxygen, O_2, to water. Electrons are taken up sequentially by the T1 copper(II) center, while dioxygen coordinates to and is reduced at the T2/T3 copper cluster. Thus, intramolecular ET is central to the function of the enzyme (54). Although no knowledge of the 3D structure was available, early results obtained by pulse radiolysis using hydrated electrons as well as the CO_2^- and reduced nitroaromatic radicals as reductants established that the T1 copper is the

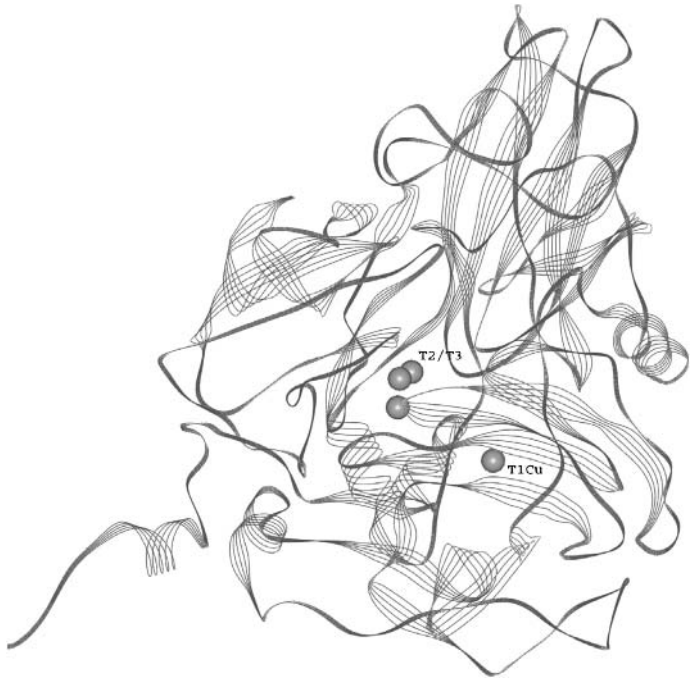

Figure 7. Three-dimensional structure of *C. pepo medullosa* ascorbate oxidase. The protein backbone is shown together with the four copper ions. Coordinates were taken from the PDB, code 1AOZ.

acceptor site (63, 64). At that time no clear evidence for intramolecular ET was presented (63). In a later study by the same group, both native AO and a modified enzyme where the T2 copper ion had been removed (T2D) were reduced pulse radiolytically using $ArNO_2^-$, CO_2^-, or O_2^- radicals (64). The reduction stoichiometry of native AO by the former agents required 6–7 equiv while for T2D only 3 equiv were necessary (all based on 610-nm absorption). Reduction by O_2^- radicals, performed in the presence of excess O_2, yielded rather limited net reduction (as expected from this experimental protocol). In contrast, T2D AO underwent full reduction of the $T1Cu^{II}$, clearly showing the requirement of an intact trinuclear center for a functional catalytic cycle (64).

Later pulse radiolysis experiments demonstrated that, following a bimolecular reduction of $T1Cu^{II}$ by the reducing radicals, $T1Cu^{I}$ reoxidation at 605 nm and concomitant $T3Cu^{II}$ reduction at 330 nm could be monitored independently and directly (48) (cf. Fig. 8). The rate of the latter reactions was independent of protein concentration, consistent with being a unimolecular process. An unprecedented feature in AO was that at least two parallel phases of intramolecular ET were resolved. For the first phase, a rate constant of $200\,s^{-1}$ was determined

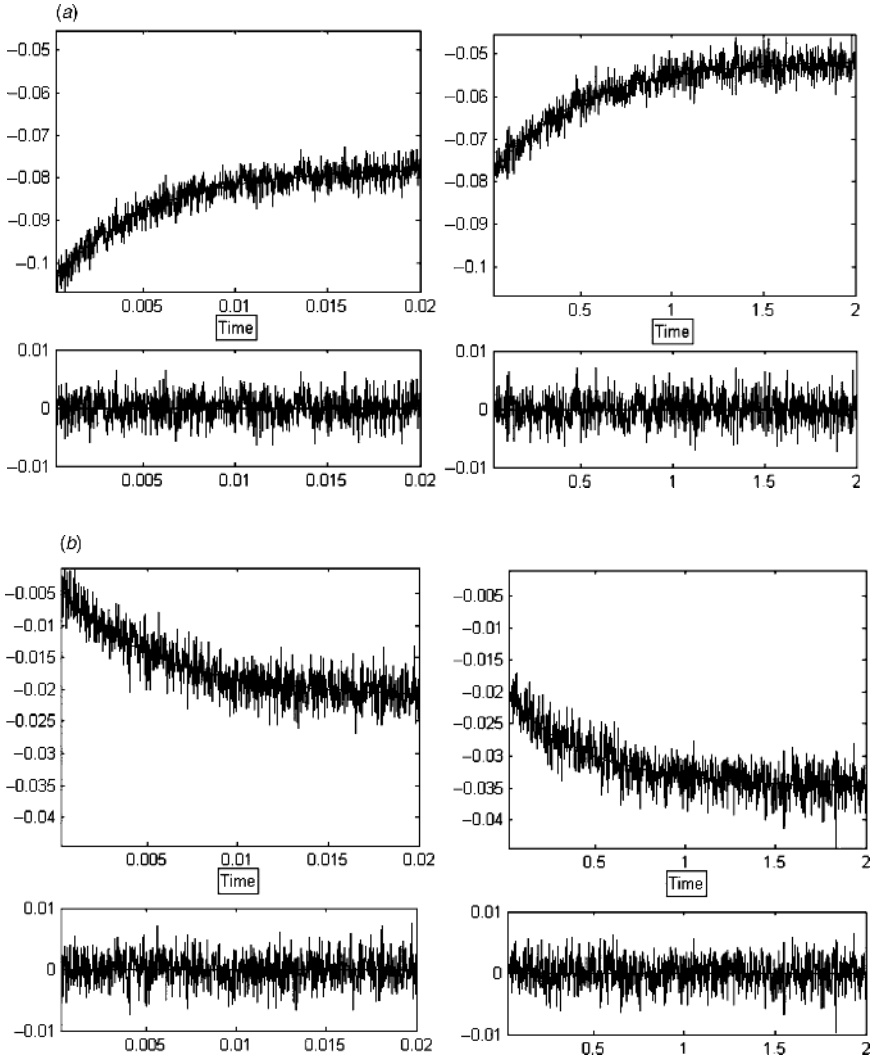

Figure 8. Time resolved absorption changes in AO following reaction with pulse-radiolytically produced CO_2^- radicals (48). (*a*) Absorption changes at 610-nm monitoring reoxidation of a 5.5-μ*M* solution of the protein by CO_2^- radicals. The initial, fast bimolecular reduction of $T1Cu^{II}$ has a half-life of $< 100\,\mu s$ and is thus not resolved on the time scales shown here. (*b*) Absorption changes at 330 nm following intramolecular reduction of the T3 copper by $T1Cu^{I}$. $T = 286\,K$; pH 5.5; 0.1 *M* formate; 10 m*M* phosphate; N_2O saturated; pulse width 1.0 μs; optical path 12.3 cm. Time is in seconds; the left panel shows the faster phase, while the right one shows the reaction taking place at the slower phase. The lower panels show residuals of the fits to the data.

at 25°C, pH 5.5 under anaerobic conditions, while a slower reaction was monitored with a rate constant of $2\,s^{-1}$ (48). The activation parameters for the faster phase are presented in Table II. Two reduction phases with similar rate constants were later reported by another group using different organic radicals as reductants, but monitoring only the 610-nm chromophore (65). The observation of two different ET processes is rather puzzling and could be rationalized by the existence of distinct conformers since the two rates can be related to differences in activation entropies (-170 ± 9 and $-215 \pm 16\,J\,K^{-1}\,mol^{-1}$, respectively), which are attributed to changes in electronic coupling between electron donor and acceptor in the two AO monomers. The observed internal ET reactions are rather slow considering that the centers are connected by a short covalent pathway with a direct distance between the T1 and the nearest T3

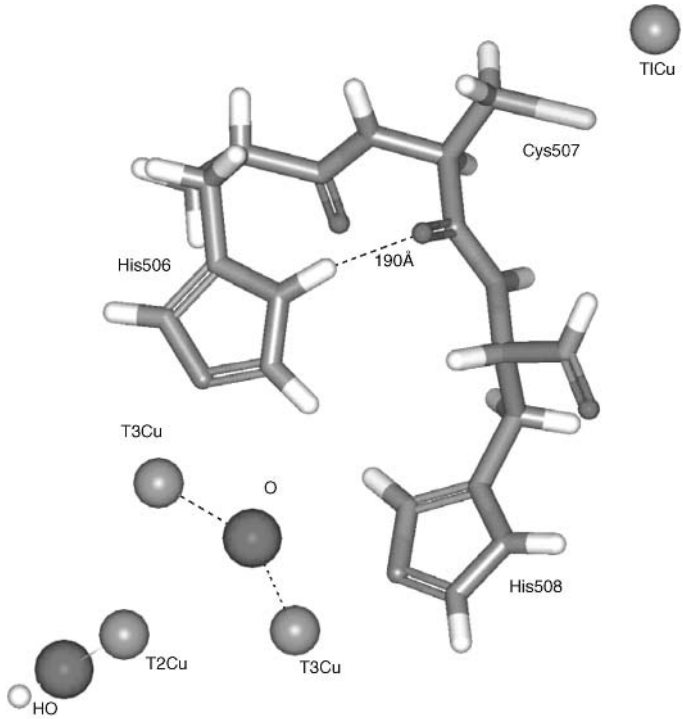

Figure 9. Electron-transfer pathways in AO. The Cys507 binds to T1, while the two neighboring residues, His506 and His508 bind to the two T3 copper ions. This provides a very short electronic coupling between Cys507 and either His506 or His508, both consisting of nine covalent bonds. An alternative pathway may be envisaged through the carbonyl oxygen atom of Cys507 and N_δ of His506. Calculations, showing that all three pathways have essentially the same electronic coupling (48), were based on the Beratan and Onuchic model (6, 7). Coordinates were taken from the PDB, code 1AOZ. (See color insert.)

copper ion of 1.2 nm (Fig. 9). One of the T1 copper ligands is a thiolate from Cys507, while imidazoles of the two neighboring histidines, His506 and His508, coordinate to the two T3 copper ions. Both pathways consist of only 11 covalent bonds. Thus, the shortest ET pathway linking the two redox centers comprise Cys507 and either His506 or His508 giving a decay factor of $\varepsilon = 3.6 \times 10^{-3}$. An alternative ET route is provided by a hydrogen bond between the carbonyl oxygen of Cys507 and His506 with an even better electronic coupling, $\varepsilon = 5.2 \times 10^{-3}$ (48). It is furhter noteworthy that similar to the azurin system discussed above the cysteine thiolate ligand takes part in ET to and from the copper ion.

A possible reason for the surprisingly slow ET processes is that the driving force is close to zero and the reorganization energy is quite large (1.5 ± 0.1 eV), suggesting that the reaction is gated either by substrate (O_2) binding or by an even larger reorganization energy of the trinuclear center due to conformational changes (48). In this context, it is interesting to compare the above rates with the rate of the initial internal Cu_A(I) to heme-*a*[Fe(III)] ET step in cytochrome *c* oxidase (COX) reduction (cf. Section V.A). While in AO the internal ET is slowed down by properties of the acceptor, this is most likely not the case in either mammalian or bacterial COX. The trinuclear copper center in AO is solvent exposed, and redox changes are expected to be accompanied by large reorganization energy requirements. In COX the electron acceptor, heme-*a*, is buried in the solvent inaccessible interior of the protein and, as shown below, the reorganization energy is quite small. This result may explain why the rate of intramolecular ET is 17,000–30,000 s^{-1}, that is several orders of magnitude faster than in the blue oxidase, although the shortest distance separating electron donor [Cu_A(I)] and heme-*a*(III) in COX is 2.0 nm through a hydrogen-bonded system, contrasting the covalent pathway distance of 1.2 nm found in AO.

Assuming that the linkage between the copper sites in the blue oxidases has been optimized by evolution, the following pertinent questions arise: (1) Is the intramolecular ET rate in AO controlled during the multielectron reduction and oxidation? (2) Does the rate of intramolecular ET depend on the number of electron equivalents taken up by the molecules? (3) Does the rate of ET relate to the conformational changes that were resolved by the structural studies? (4) Finally, how can the turnover number of the enzyme, determined under steady state conditions (12,000–14,000 s^{-1}), be considerably faster than the above rate of intramolecular ET? Since AO molecules reduced to different degrees (from 0–95%) yielded identical ET rates, the notion that the rate depends on the number of electron equivalents taken up can be rejected (48). Also, enzymes that have been activated or pulsed by going through a turnover of 1 m*M* ascorbate and 0.25-nm O_2 prior to the PR experiment did not show different rates of internal ET. However, in a study where a controlled small amount of dioxygen (15–65 μ*M*) was introduced into the solution, a conspicuous difference in reactivity was observed (66). A new and faster phase of intramolecular ET

was discovered with a rate constant of $1100\,s^{-1}$ (18°C, pH 5.8), which was maintained as long as O_2 remained in the solution. At the same time, large spectral changes took place, most probably due to interaction between O_2 and the partially reduced T2/T3 center. Dioxygen or its reduction intermediates coordinated to the trinuclear center would most probably increase the driving force of ET considerably and cause the observed increase in rate of intramolecular ET. Still, it is unclear whether the first species interacting with O_2 are partially reduced AO molecules or whether the fully oxidized enzyme is capable of such binding (66). Calculations show that an increase in driving force of 0.1 eV would suffice to produce the observed fivefold increase in rate. However, as this increase does not account for the experimentally observed turnover, an interaction between AO and O_2 is not adequate for attaining maximal enzymatic activity. Under optimal physiological conditions, the concentration of the reducing substrate, ascorbate, is sufficient for maintaining a steady state of fully reduced copper centers, an observation that was exploited in a flash photolysis study where reoxidation of fully reduced AO was followed using a laser generated triplet state of 5-deazariboflavin as electron acceptor (67). Subsequent to the assumed one-electron oxidation of the T2/T3 center, rapid electron transfer from $T1Cu^I$ and (presumably) to the trinuclear center was monitored with a rate constant of $\sim 10,000\,s^{-1}$, which is comparable to the turnover rate, so it is possible that this is the rate-limiting step in catalysis. Why this fast internal ET process could not be resolved in the PR studies of the oxidized enzyme remains unclear.

2. *Ceruloplasmin*

Mammalian ceruloplasmin (Cp) is an exceptional case among the blue copper oxidase family members for several reasons: First and foremost, its function as an oxidase has been a subject of considerable debate for a long time; though its capacity to catalyze ferrous ion oxidation by dioxygen has been well established and its involvement in iron metabolism strongly supported by considerable physiological and genetic evidence, only recently has its physiological function as a ferroxidase been fully accepted (68). Another conspicuous characteristic is the copper content, and hence the number and nature of possible active sites, topics that have been debated for quite some time. The 3D structure determination of human Cp (hCp) clearly resolved the latter issue by revealing the presence of three distinct T1 sites in addition to a single trinuclear cluster (59) (cf. Fig. 10). Finally, Cp is the only known mammalian member of the blue copper protein family.

The more recent advances in understanding copper and iron homeostasis are based to a large extent on studies of ferroxidase in lower organisms. In yeast, a correlation between the ferroxidase activity and a high-affinity iron uptake

complex has been demonstrated. Further, the ferroxidase present in *Saccharomyces cerevisiae*, Fet3p, has been extensively studied and its 3D structure was recently determined (60).

Human ceruloplasmin consists of a single polypeptide chain with a MW of 132 kDa folded in six cupredoxin domains arranged in a triangular array. Each domain comprises a β-barrel, constructed in a Greek key motif, typical for the cupredoxins. Three of the six copper ions are bound to T1 sites present in domains 2, 4, and 6, whereas the other three copper ions form a trinuclear cluster, bound at the interface between domains 1 and 6 (Fig. 10). The spatial relation between the trinuclear center and the nearest T1 site (A, in domain 6) closely resembles that found in AO and was taken to further support the proposal that hCp has an oxidase function. The three T1 sites are separated from each other by a distance of 1.8 nm, a distance that might still allow for internal ET at reasonable rates and could also increase the probability for electron uptake. The coordination sphere of the T1 site in domain 4 (T1B) is identical with that of domain 6 (T1A). The third type 1 center (T1C), however,

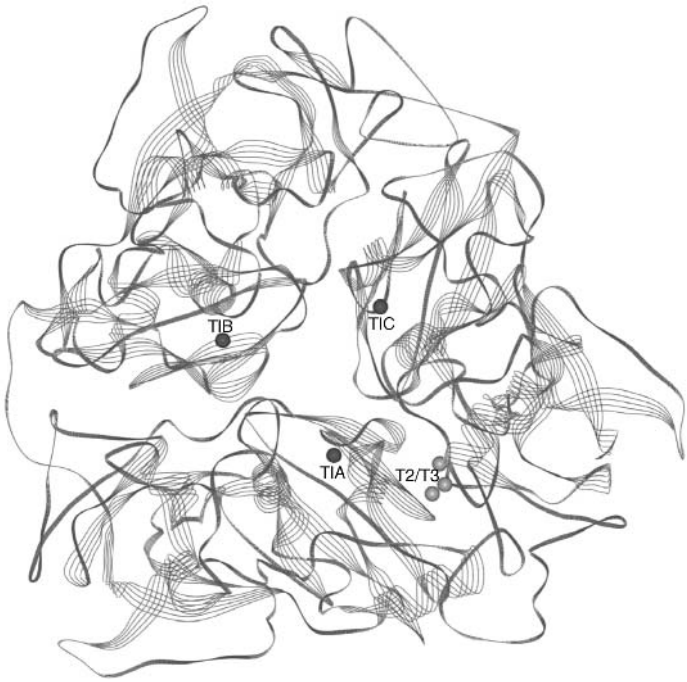

Figure 10. The 3D structure of human Ceruloplasmin. The protein backbone is shown together with the three T1 copper ions and the trinuclear T2/T3 site. Coordinates were taken from the PDB, code 1KCW.

contains a nonligating Leu residue instead of the ''usual'' Met. Redox titrations along with EPR and UV–VIS (visible) spectroscopy demonstrated that hCp contains three paramagnetic copper(II) ions, two in T1 sites and one in a T2 center (69). In analogy with ascorbate oxidase, two of the copper ions in the trinuclear site are bound to six histidines and assigned as the T3 site, while the third copper (most distant from T1) is coordinated to two histidines only, and is designated as the T2 site. By further analogy to the ascorbate oxidase structure, an oxygen atom connects the two T3 coppers, while another is bound to the T2 copper ion. An additional relevant structural feature is the domain 6 cysteine (Cys1021) that provides the thiolate ligand to the T1 site; it is placed between the neighboring histidine residues (His1020 and His1022) coordinated to the T3 copper pair (59). As in ascorbate oxidase, this sequence motif most likely provides the ET path between T1 and the trinuclear center (cf. Fig. 9).

The 3D structure of hCp further resolved five disulfide bridges distributed evenly throughout the protein in domains 1–5. All five disulfides are near the bottom of a β-barrel, and in two domains the T1 copper centers (T1B and T1C) are placed at the opposite end of the barrel. The only domain lacking a disulfide is domain 6, which contains T1A and the trinuclear copper centers.

The reduction potentials of two of the T1 copper centers were determined to be 580 and 490 mV, respectively (69). However, the experimental accuracy did not allow for a precise determination of whether hCp contains three or four nonparamagnetic copper ions. For azurin, where the copper ligating Met was substituted by Leu or Val, the T1 copper reduction potentials were found to increase from 307 to 412 to 445 mV (WT $<$Leu $<$Val) at pH 7.0 (39). Moreover, X-ray absorption spectroscopy suggested that the resting oxidized enzyme contains one permanently reduced T1 center, and that this site cannot be involved in the catalytic process, since its reduction potential is at least 1.0 V (70). Thus, based on the above electrochemical results and the 3D structure of hCp, this high-potential T1 site can be assigned to T1C of domain 2 (Fig. 10). Recently, the 3D structure determination of fungal laccase from *Trametes versicolor* has shown that a phenylalanine residue replaces methionine in the strongly oxidizing T1 copper(II) center (61).

A considerable body of results accumulated during earlier decades from activity studies of hCp now awaits a more meaningful analysis using the available 3D structure. Catalysis of amine oxidation by hCp, in particular biogenic ones present in plasma, cerebral, spinal, and intestinal fluids as well as of ferrous ions, which is probably physiologically relevant, has been studied extensively (68, 71). The mechanism of dioxygen reduction by hCp at the trinuclear center is of particular interest, as the presence of three distinct T1 sites raises the question of which centers are involved in internal ET to the single O_2 reduction site. This mechanistic question prompted us to initiate ET studies by PR.